Mon. Not. R. Astron. Soc. **000**, 1–16 (2012) Printed 8 November 2018 (MN LaTeX style file v2.2)

The star formation history of the Large Magellanic Cloud star clusters NGC 1846 and NGC 1783 ⋆

Stefano Rubele[1], Léo Girardi[1], Vera Kozhurina-Platais[2], Leandro Kerber[3], Paul Goudfrooij[2], Alessandro Bressan[4], Paola Marigo[5]

[1] *Osservatorio Astronomico di Padova – INAF, Vicolo dell'Osservatorio 5, 35122 Padova, Italy*
[2] *Space Telescope Science Institute, 3700 San Martin Drive, Baltimore, MD 21218, USA*
[3] *Universidade Estadual de Santa Cruz, Rodovia Ilhéus-Itabuna, km. 16 – 45662-000 Ilhéus, Bahia, Brazil*
[4] *SISSA, via Bonomea 265, 34136 Trieste, Italy*
[5] *Dipartimento di Fisica e Astronomia, Università di Padova, Vicolo dell'Osservatorio 2, 35122 Padova, Italy*

arXiv:1301.3381v1 [astro-ph.SR] 15 Jan 2013

Accepted ... Received ...;

ABSTRACT

NGC 1846 and NGC 1783 are two massive star clusters in the Large Magellanic Cloud, hosting both an extended main sequence turn-off and a dual clump of red giants. They present similar masses but differ mainly in angular size. Starting from their high-quality ACS data in the F435W, F555W and F814W filters, and updated sets of stellar evolutionary tracks, we derive their star formation rates as a function of age, SFR(t), by means of the classical method of CMD reconstruction which is usually applied to nearby galaxies. The method confirms the extended periods of star formation derived from previous analysis of the same data. When the analysis is performed for a finer resolution in age, we find clear evidence for a $\sim$ 50-Myr long hiatus between the oldest peak in the SFR(t), and a second prolonged period of star formation, in both clusters. For the more compact cluster NGC 1846, there seems to be no significant difference between the SFR(t) in the cluster centre and in an annulus with radii between 20 and 60″ (from 4.8 to 15.4 pc). The same does not occur in the more extended NGC 1783 cluster, where the outer ring (between 33 and 107″, from 8.0 to 25.9 pc) is found to be slightly younger than the centre. We also explore the best-fitting slope of the present-day mass function and binary fraction for the different cluster regions, finding hints of a varying mass function between centre and outer ring in NGC 1783. These findings are discussed within the present scenarios for the formation of clusters with multiple turn-offs.

Key words: Stars: evolution – Hertzsprung-Russell (HR) and C-M diagrams

1 INTRODUCTION

The star clusters NGC 1846 and NGC 1783 represent prototypes of massive intermediate-age star clusters in the LMC containing multiple main sequence turn-offs (MMSTO; Mackey & Broby Nielsen 2007; Mackey et al. 2008; Milone et al. 2009; Goudfrooij et al. 2009). They have masses of about 1.5 and 1.7×10^5 $M_\odot$, respectively, which locates them among the most massive LMC clusters except for the old globulars (see e.g. fig. 13 in Girardi et al. 1995). In addition to the MMSTOs, they also seem to present a dual clump of red giants, in similarity to the SMC cluster NGC 419 (Girardi, Rubele & Kerber 2009) and the LMC's NGC 1751 (Rubele et al. 2011).

The presence of MMSTOs is commonly interpreted as the signature of continued star formation, or multiple events of star formation, spanning a few 100 Myr in time (e.g., Mackey & Broby Nielsen 2007; Mackey et al. 2008; Goudfrooij et al. 2009, 2011a; Conroy & Spergel 2011; Girardi, Eggenberger & Miglio 2011; Keller, Mackey & Da Costa 2011)[1]. For a well-

⋆ Based on observations with the NASA/ESA *Hubble Space Telescope*, obtained at the Space Telescope Science Institute, which is operated by the Association of Universities for Research in Astronomy, Inc., under NASA contract NAS5-26555

[1] The dispersion in rotational velocities in a coeval cluster, advocated by Bastian & de Mink (2009), was shown by not to produce MMSTOs similar to the observed ones, both theoretically (Girardi, Eggenberger & Miglio 2011) and observationally (see

© 2012 RAS

defined age range between 1.2 and 1.7 Gyr, star clusters with a turn-off age spanning a few 100 Myr will temporarily contain stars that ignited helium under both non-degenerate and degenerate conditions, and hence naturally develop a dual red clump (Girardi, Rubele & Kerber 2009).

The main difficulties with the prolonged-star formation history (SFH) interpretation of MMSTOs, are related with the theories of star formation and gas dynamics inside the relatively shallow potential wells of star clusters. Conroy & Spergel (2011) and Goudfrooij et al. (2011a) describe scenarios for the continuation of star formation over long timescales which imply that more massive clusters may have more extended SFHs. Conroy & Spergel (2011) specifically note that all clusters with MMSTOs have masses higher than $\sim 10^4$ $M_\odot$, whereas Goudfrooij et al. (2011a) find a correlation between the estimated escape velocities at an age of 10 Myr and the concentration of stars in the brightest half of the MMSTO region. Moreover, Keller, Mackey & Da Costa (2011) notice the correlation between the cluster core radius r_c and their SFHs, in the sense that all known clusters with MMSTOs have $r_c >$ 3.7 pc. Further testing these trends, and finding additional correlations with other cluster parameters, are probably necessary steps to clarify the origin of clusters with MMSTOs.

In this context, the pair of clusters NGC 1846 and NGC 1783 is extremely interesting. While they have very similar total masses ($\log(M/M_\odot) = 5.17 \pm 0.09$ and 5.25 ± 0.09, respectively; Goudfrooij et al. 2011b) and mean ages (1.73 ± 0.10 and 1.70 ± 0.10 Gyr, respectively; Goudfrooij et al. 2011a), and a similar location in the Northwest portion of the LMC (hence similar fore/background, and likely the same distance), they have very different angular sizes: for NGC 1846 the core radius is $r_c = 26.0'' =$ 6.3 pc, and the concentration index $c = r_t/r_c$ (where r_t is the tidal radius) is 6.2 (Goudfrooij et al. 2009); for NGC 1783 these quantities are $r_c = 37.7'' = 9.1$ pc and $c = 9.2$ (Goudfrooij et al. 2011b), respectively[2]. So, in these clusters we can test whether there is any measurable difference in their SFHs that can be interpreted as a result of the different radii, and in the light of the correlation noted by Keller, Mackey & Da Costa (2011).

In this paper, we examine the SFHs of NGC 1846 and NGC 1783 using the same CMD reconstruction method previously applied to NGC 419 and NGC 1751 (Rubele, Kerber & Girardi 2010; Rubele et al. 2011). This method is significantly different from other analyses of the same clusters that appeared in the literature (Mackey & Broby Nielsen 2007; Mucciarelli et al. 2008; Mackey et al. 2008; Milone et al. 2009; Goudfrooij et al. 2009, 2011a), which concentrate on the MSTO region of the CMD. The CMD reconstruction method finds the best-fitting model for the entire CMD above a given magnitude cut, without giving particular weight to any subset of the observed stars. As such, it may be more affected by errors in evaluating the contribution from field stars or the photometric errors of faint stars – aspects that, in any case, are taken into account in the method. On the other hand, by using the entire available data set, the CMD reconstruction method potentially enhances the statistical significance of the detected SFH features. This is important considering that the number of stars along the MMSTOs is anyway limited to a few hundreds, even for the most populous LMC clusters. Moreover, this aspect might be crucial in the analysis of less populous clusters.

In the following, we will use the excellent imaging and photometry of NGC 1846 and NGC 1783 available from HST/ACS, together with new sets of evolutionary tracks and isochrones (Sect. 2). Sect 3 will apply the CMD reconstruction method of SFH-recovery to the surrounding NGC 1846 and NGC 1783 LMC fields (Sect. 3.2) and cluster areas (Sect. 3.3). Sect. 4 discusses the results in the framework of present scenarios for the formation of MMSTOs.

2 THE DATA

2.1 Cluster imaging and photometry

The data set used in this paper comes from GO-10595 (PI: Goudfrooij), and consists of one short and two long exposures in F435W, F555W, and F814W with small dither patterns to avoid the gap between two ACS/WFC chips. A detailed description of the observations and photometry is given in Goudfrooij et al. (2009) and Goudfrooij et al. (2011b). Nevertheless, in this paper we use the simultaneous ePSF fitting technique as it described in Anderson et al. (2008), which fits the PSF simultaneously on all exposures/observations of the cluster. Differently from Goudfrooij et al. (2009), the Charge Transfer Efficiency (CTE) correction was performed using Riess & Mack (2004) formula (ACS-ISR 2005). The derived photometry was calibrated into the Vegamag system as described in Goudfrooij et al. (2009).

The left panels in Figs. 1 and 2 show the spatial representation of the stars we analyse in this work, for the two clusters. The right panels show how the stellar density varies as a function of radius from the NGC 1846 and NGC 1783 centres, taking into account only the stars of $F814W < 22$, for which the photometry is nearly complete. Based on these figures, we define Centre and Ring regions having radii and areas as tabulated in Table 1. For both clusters, the Centre regions have radii very close to the measured core radii r_c. The Ring external radii are selected to be three times the Center radii (or about $3 \times r_c$), which include at least twice the number of stars as in the Centre regions. The figures also indicate the flattening of the stellar density for radii $r \gtrsim 2700$ pix, which probably represents the regions which start being dominated by LMC field rather than by cluster stars. These radii were chosen as the inner boundary of

the recent observations of the open cluster Tr 20 by Platais et al. 2012).

[2] The tidal radius and concentration index of NGC 1783 are not well constrained from the ACS/WFC data alone, due to its large radius. Its large r_c, instead, is well constrained and evident even from a simple visual inspection of the HST ACS/WFC images used by Goudfrooij et al. (2009). We note that there are two previous fits of King profile to NGC 1783 in the literature, both providing smaller values of r_c: Elson (1992) finds $r_c = 4.9$ pc $= 20''$ using ground-based data, while Mucciarelli, Origlia & Ferraro (2007) find $r_c = 24.5''$ from the shallower ACS/WFC images from SNAP 9891 (PI: G. Gilmore). These small values probably explain why, in figure 3 of Keller, Mackey & Da Costa (2011), NGC 1846 and NGC 1783 appear as if they had the same r_c, which is not correct.

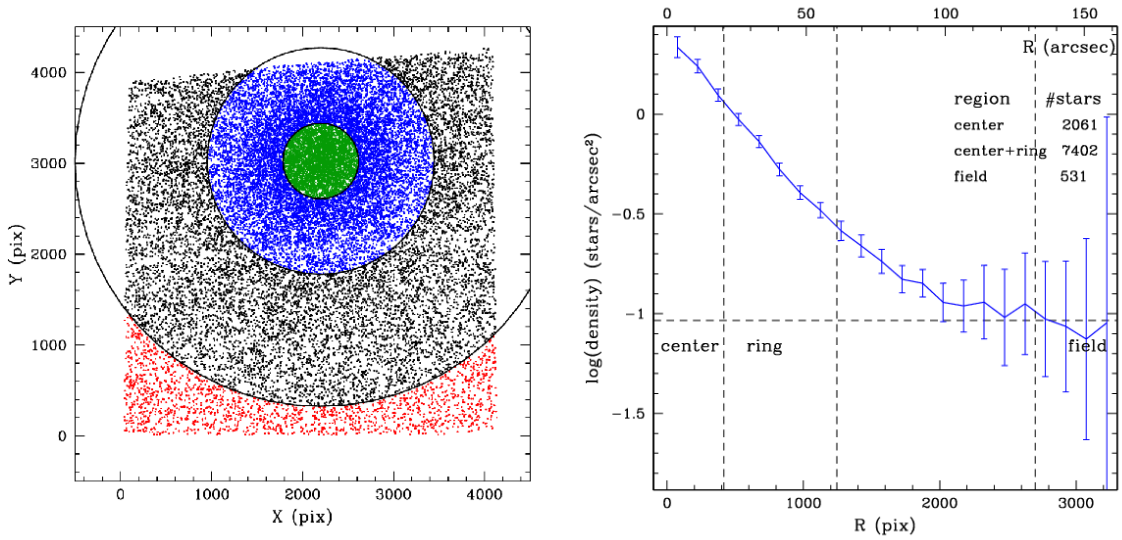

Figure 1. Left panel: Map of the stars used in this work, in the xy plane of the ACS/WFC images of NGC 1846. The scale is of about $0.05''$/pix. The observed stars have been grouped in areas corresponding to the LMC field (red) and, for NGC 1846, an inner "Centre" (green) and outer "Ring" (blue). **Right panel:** The logarithm of stellar density as a function of radius from the NGC 1846 centre. Error bars are the random errors. In the top right corner we indicate the total numbers of stars used to build the profile, selected at F814W < 22 mag.

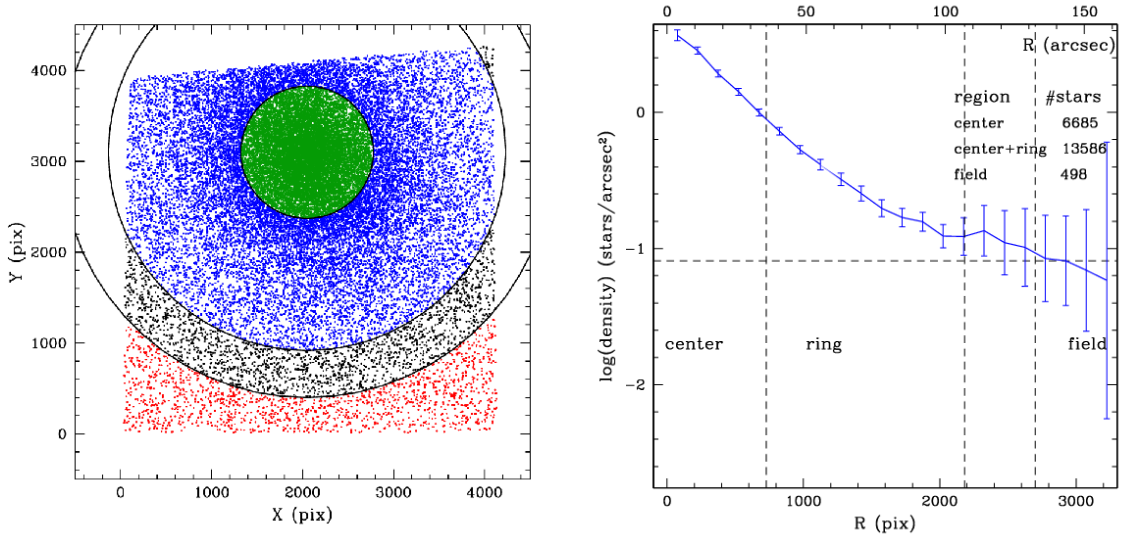

Figure 2. The same as Fig. 1, but for NGC 1783.

the LMC Field for each cluster. Although these Field radii are poorly defined – especially for NGC 1783 – their stellar densities are clearly very small compared to the Centre and Ring regions. The field stellar densities are also similar, as expected for clusters located in the same portion of the LMC.

Fig. 3 shows the ACS data for the different regions of NGC 1846 and NGC 1783, in the F814W vs. F435W–F814W and F814W vs. F555W–F814W CMDs. These plots will be used as a reference in our analysis.

The CMDs for the clusters show very clearly the broad main sequence turn-off, the composite structure of the red clump, and other well-known CMD features such as the sequence of binaries parallel to the main sequence, and the RGB, subgiants, and early-AGB bump. A simple comparison between the CMDs for the Centre and Field reveals that the field contamination in the Centre of both clusters is close to negligible. Indeed, the stellar densities in the Fields are about 25 times smaller than in the cluster Centres (see last column of Table 1). Notwithstanding, it appears evident that the Field region in NGC 1783 is marked by a population with about the same turn-off as the cluster, which is probably indicating that areas dominated by the "pure LMC field" have not been reached in this case. We will evaluate the impact of this possibility further down in our analysis.

Table 1. Selected regions. The last 2 columns refer to stars with $F814W < 22$ mag.

Region	radii		area	# stars	mean density
	($''$)	(pc)	(arcmin^2)		(arcsec^{-2})
NGC 1846 Centre	$r < 20$	$r < 4.8$	0.380	2081	1.52
NGC 1846 Ring	$20 < r < 60$	$4.8 < r < 15.4$	2.806	5321	0.527
NGC 1846 Field	$r > 133$	$r > 32.2$	2.454	531	0.060
NGC 1783 Centre	$r < 33$	$r < 8.0$	1.141	6685	1.63
NGC 1783 Ring	$33 < r < 107$	$8.0 < r < 25.9$	6.742	6901	0.284
NGC 1783 Field	$r > 133$	$r > 32.2$	2.212	498	0.063

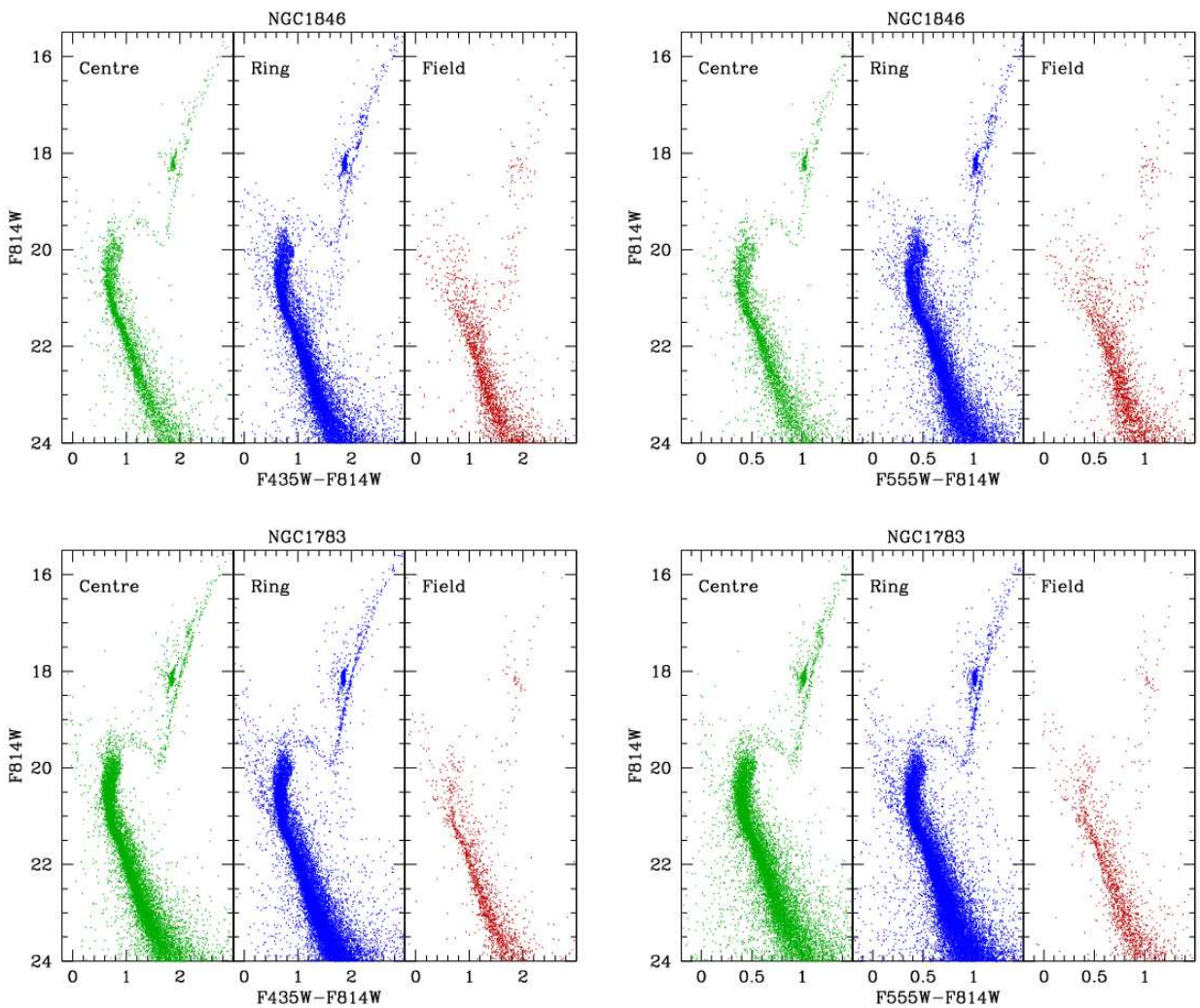

Figure 3. CMDs for NGC 1846 and NGC 1783. The selected regions are the same illustrated in Figs. 1 and 2.

2.2 Assessing photometric errors and completeness

In order to characterize the errors in the photometry and the completeness of the sample, we have performed a series of artificial star tests (AST) on the reduced images (see e.g. Gallart et al. 1999; Harris & Zaritsky 2001). The procedure consists of adding stars of known magnitude and colour at random places in each exposure, and redoing the photometry exactly in the same way as described in Sect. 2.1. The artificial stars are considered to be recovered if the input and output positions are closer than 0.5 pixels, and flux differences are less than 0.5 mag. In order to avoid the introduction of additional crowding in the images, artificial stars are positioned at distances much higher than their PSF width. So, our AST are distributed on a grid spaced by 20 pix, which is each time randomly displaced over each set of exposures. Importantly, the AST tests are repeated many more times in the central cluster regions, in numbers which are proportional to the density of stars brighter than

F814W < 22.5 mag. In this way, we have a better description of the errors in the most crowded cluster regions, and are able to accurately describe their decrease with the radial distance from the centre.

A total of 5.2 million ASTs were performed, with colors and magnitudes covering in an almost uniform way the CMD area of the observed stars and of the "partial models" to be used in the SFH analysis (see Sect. 3.1 below). For the cluster centres, the 90 % completeness limit turns out to located at F814W ~ 24.5, which is well below the position of the MMSTOs in both NGC 1846 and NGC 1783, as can be seen in Fig. 3.

2.3 Stellar models

An additional goal of this paper is to employ a new set of evolutionary tracks derived from the PAdova & tRieste Stellar Evolution Code (PARSEC) and extensively described in Bressan et al. (2012). They include updated input physics (opacities, equation of state, neutrino losses, etc.), and revised prescriptions for the convective processes, including microscopic diffusion in low-mass stars and an excellent description of helioseismic data. These improvements are expected to provide a more detailed description of CMD features and a more robust age scale than previous versions of Padova tracks. In the mass interval of interest for this work, overshooting is assumed to operate with an efficiency of $\Lambda_c = 0.5$ pressure scale heights (cf. Bressan, Chiosi & Bertelli 1981).

The initial chemical composition is derived from the Caffau et al. (2011) new solar composition after enhancing the abundances of α elements by +0.2 dex. This mild α enhancement has just a minor effect in the shape of evolutionary tracks and isochrones, but it is necessary to reproduce the chemical composition of AGB stars observed in NGC 1846 by Lebzelter et al. (2008), as will be discussed in Marigo et al. (in prep.).

The stellar evolutionary tracks are transformed into isochrones and converted to the ACS/WFC Vegamag photometric system using the transformations described in Girardi et al. (2008).

3 RECOVERING THE SFH

3.1 Overview of the method

To recover the SFH from the ACS data, we use the same method applied to the SMC star cluster NGC 419 (Rubele, Kerber & Girardi 2010) and later improved with the LMC cluster NGC 1751 (Rubele et al. 2011): We use the StarFISH code (Harris & Zaritsky 2001, 2004) to look for the linear combination of "stellar partial models" (SPM) that best-fits the Hess diagram[3] of the observations, via the minimization of a χ^2-like statistics (cf. Dolphin 2002). The coefficients of this best-fit linear combination directly translated into the SFH, and can be plotted in different ways – for instance, as the star formation rate as a function of age, SFR(t), plus the age–metallicity relation (AMR), [Fe/H](t).

[3] The Hess diagram is simply a representation of the stellar density – number of stars per color–magnitude bin – across the CMD.

SPMs are the basic building blocks in the method. They are theoretically-derived Hess diagrams of simple stellar populations spanning very small ranges of age and metallicity. They are initially produced in a purely theoretical way, with the aid of the TRILEGAL population synthesis code (Girardi et al. 2005) and the PARSEC stellar evolutionary tracks. Then, these "perfect" SPMs are displaced by the distance modulus and reddening to be tested, and degraded using the distributions of incompleteness and photometric errors as derived from the ASTs. Specifically, all ASTs falling in the spatial region under consideration, and for each small box in the CMD, are grouped together and used to derive the two-dimensional error and completeness distributions, that then are used to blur the same boxes in the theoretical SPMs. Examples of this procedure are presented in figure 4 of Rubele, Kerber & Girardi (2010) .

In the case of star clusters, our customized version of StarFISH performs the following steps:

(i) For each set of ACS frames, we first recover the best-fitting SFH of the Field region, exploring different values of A_V and $(m-M)_0$, as described in Sect. 3.2.

(ii) From this best fitting solution and our set of stellar models, we generate a Field Stellar Partial Model (FSPM). This special partial model is (a) scaled to the cluster area to the analysed, and (b) degraded using the ASTs performed *in* the cluster area. Finally, this FSPM is included as a fixed component during the SFH-recovery of the Center and Ring regions. In this way, the SFH-recovery of the cluster area includes the best possible estimate for the LMC field contamination.

(iii) We perform the SFH-recovery of the cluster area exploring a wide range of extinction, distant modulus, and metallicity values (Sect. 3.3).

(iv) This process is initially performed assuming a single value of binary fraction f (for binaries with mass ratios in the range between 0.7 and 1.0), and a fixed present-day mass function (PDMF) from Chabrier (2001). Variations in these parameters are later explored. The default value of f is 0.3 for the LMC field, and 0.2 for the star clusters (cf. sect. 4.1 in Rubele et al. 2011).

For the specific case of our NGC 1846 and NGC 1783 data, we will use the entire CMD regions above F814W $<$ 22.5 mag. This ensures that we will be dealing with near-complete CMDs including all main sequence turn-offs up to the oldest possible ages.

3.2 The SFH in the LMC Fields

Deriving the SFH in the LMC fields is not a main goal in this paper, but it is both an interesting side-product of the present analysis, and a necessary step to reduce systematic errors in the cluster SFH.

For both the NGC 1846 and NGC 1783 Fields, we derive the SFH using the same set of SPMs as defined in Rubele et al. (2011). We then run StarFISH to find the best-fitting solution to the observed CMDs, for a given value of distance modulus $(m-M)_0$ and extinction A_V. Both F814W vs. F435W–F814W and F814W vs. F555W–F814W Hess diagrams are used simultaneously in the process of χ^2 minimization.

Figure 4 shows the map of $\chi^2_{\rm min}$ – that is, the χ^2 value

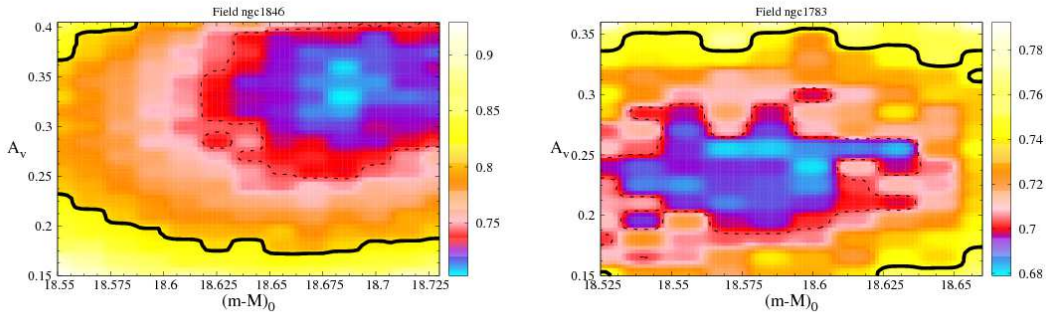

Figure 4. χ^2 map for the Field best-fitting solutions, as a function of distance modulus and V-band extinction. The dashed and continuous black line show the 68 % and 95 % confidence levels for the overall best-fitting solution. The best-fitting model is located at $(m-M)_0 = 18.685, A_V = 0.33$ for the NGC 1846 Field (**left panel**), and at $(m-M)_0 = 18.60, A_V = 0.225$ for the NGC 1783 Field (**right panel**).

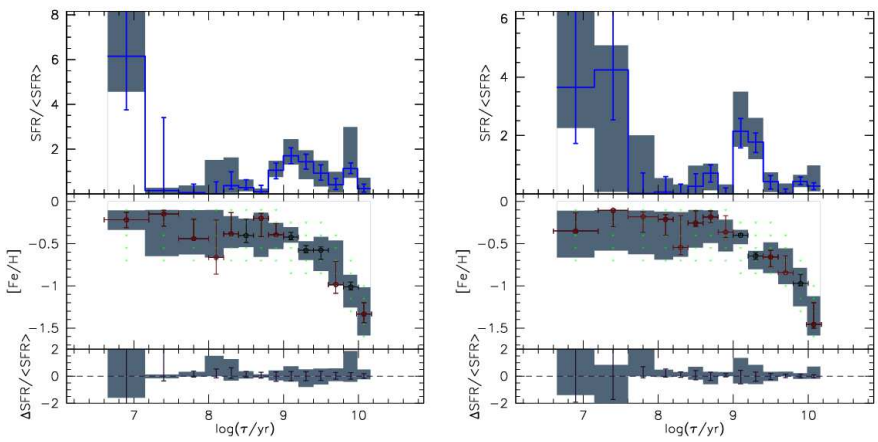

Figure 5. The SFH derived for the NGC 1846 and NGC 1783 Fields (**left and right panels**, respectively). In both cases, the **top panel** presents the best-fitting SFR(t) for the field (blue histogram), together with the random errors (1σ blue bar) and systematic errors (gray shadow) as estimated from the entire 68 % confidence level interval in the $(m-M)_0, A_V$ plane. The **bottom panels** present the mean age–metallicity relation (red and black point) with stochastic errors (red and black) and systematic errors (shaded regions). The green points show the center of distributions of the SPMs used to derive the SFH.

to which StarFISH converges – for the solutions in the $(m-M)_0 \times A_V$ plane. We explored a range in both parameters just extended enough to allow a clear identification of the absolute minimum and most of its 68 % confidence level interval. There are a couple of remarkable aspects in our results.

First, the best-fitting models for the NGC 1846 and NGC 1783 Fields (left and right panels of Fig. 4, respectively) present quite a different mean extinction, with $A_V = 0.33$ mag and $A_V = 0.225$ mag, respectively. In comparison, for a radius of 12 arcmin around the clusters NGC 1846 and NGC 1783, Zaritsky et al. (2004) derive extinction values of $\langle A_V \rangle = 0.59 \pm 0.40$ and $\langle A_V \rangle = 0.41 \pm 0.42$, respectively ($\langle A_V \rangle = 0.48 \pm 0.32$ and $\langle A_V \rangle = 0.31 \pm 0.26$ for cool stars). The reddening maps by Haschke, Grebel & Duffau (2011) cover only the region of NGC 1846, providing $\langle E_{V-I} \rangle \geqslant 0.06 \pm 0.075$, which translates into $\langle A_V \rangle \gtrsim 0.14$ mag. Considering the errors and the large dispersion in extinction values, all these values are consistent with each other.

Second, the best-fitting distances for both fields just marginally agree one with each other, considering their 68 % confidence level: indeed the distance modulus of $(m-M)_0 \sim 18.625$ mag represents, at the same time, a lower limit to the distance of the NGC 1846 field, and an upper limit to the distance of the NGC 1783 one. Although these distance measurements are perfectly compatible when we consider their 95 % confidence levels, we cannot refrain from noticing this unexpected result. Both fields have similar location in the Northwest portion of the LMC, relatively close to the line of nodes of the LMC disk. So, according to recent results for the LMC disk geometry (e.g. van der Marel & Cioni 2001; van der Marel et al. 2002; Nikolaev et al. 2004; Rubele et al. 2012), they would be expected to have the same distance of the LMC center (of $(m-M)_0 \sim 18.46$ mag, see Ripepi et al. 2012 and references therein). Although the relative distances between the cluster fields and the LMC centre could be affected by systematic errors, the relative distances between both cluster fields should be quite solid.

We note however that both the distances and extinction values for the field populations are consistent, within

their 1σ uncertainties, with the values found for the cluster centres, as detailed in the next subsection.

Finally, Fig. 5 presents the SFR(t) and AMR corresponding to the best-fitting solutions for both Fields. It is remarkable that the SFR(t) recovered for the NGC 1846 Field presents features that are consistent with those commonly found in previous works, based on both HST (Olsen 1999; Holtzman et al. 1999; Smecker-Hane et al. 2002; Javiel, Santiago & Kerber 2005) and ground-based data (Harris & Zaritsky 2001, 2009; Rubele et al. 2012). There is an initial period of star formation at ~ 10 Gyr, followed by a minimum at $\log(t/\mathrm{yr}) \simeq 9.7$, and then a more extended period of star formation for ages between about 1 and 4 Gyr. For younger ages, our data includes too small an area to set stringent constraints on the SFH; however, there are hints for significant SFR at ages of about 300 Myr ($\log(t/\mathrm{yr}) = 8.5$), and a well detected burst of formation of stars with ~ 10 Myr ($\log(t/\mathrm{yr}) = 7.0$). Error bars are too large to allow a meaningful quantitative comparison with the results from Harris & Zaritsky (2009) and Rubele et al. (2012), for nearby regions of the LMC.

The SFR(t) for the NGC 1783 Field, instead, presents a marked "burst" at ages between 1 and 2 Gyr, which, as we will see later, coincides with the ages of cluster formation. This is a further evidence that in NGC 1783 Field we are still sampling the cluster population.

Concerning the AMR, the results for the NGC 1846 and NGC 1783 fields are quite similar and consistent with those derived from LMC star clusters (Kerber, Santiago & Brocato 2007; Harris & Zaritsky 2009) and for the LMC field using different sets of data (e.g. Carrera et al. 2008; Rubele et al. 2012).

3.3 The SFHs in NGC 1846 and NGC 1783

For NGC 1846 and NGC 1783 we proceed deriving the best-fitting SFH in the same way as performed for NGC 1751 (Rubele et al. 2011). In these cases, we assume that cluster stars present the same mean [M/H] value for all ages, since so far there is no evidence for significant spreads in metallicity in such star clusters (e.g. Mucciarelli et al. 2008; Rubele, Kerber & Girardi 2010; Rubele et al. 2011). We have explored seven [M/H] values: -0.57, -0.54, -0.52, -0.49, -0.47, -0.44, -0.42. For each one of these mean [M/H] values, a box-shaped metallicity distribution is assumed, with a total width of Δ[M/H] $= 0.025$ dex. This spread is similar to the separation between the mean [M/H] values, and contributes to produce results that vary smoothly as a function of metallicity.

The age interval covered by our SPMs goes from $\log(t/\mathrm{yr}) = 8.9$ to 9.4, which is much wider than the interval suggested by the position of NGC 1846 and NGC 1783 MMSTOs. We initially adopt an age resolution (bin width of SPMs) of $\Delta \log t = 0.05$ dex. So, for each set of parameters, we have a total of 11 partial models – 10 for the cluster, plus the FSPM described in Sect. 3.1 – completely encompassing the age interval of interest.

3.3.1 The SFH for the NGC 1846 Centre

Complete maps of $\chi^2_{\rm min}$ for the NGC 1846 Centre, as a function of $(m-M)_0$, A_V and metallicity, are presented in the first seven panels of Fig. 6. These results are obtained for the age resolution of $\Delta \log t = 0.05$ dex. We can notice that the best solutions are found in the metallicity interval between [M/H] $= -0.52$ and -0.42. The last panel shows the same kind of map for the Ring, but limited to the metallicity that provides the best fit for the Centre, namely [M/H] $= -0.49$. This value is in excellent agreement with the one derived from the Ca II triplet of cluster members by Grocholski et al. (2006).

The best solution for the Centre is for $(m-M)_0 = 18.57, A_V = 0.26$, with a $\chi^2_{\rm min} = 0.55$. Such a small $\chi^2_{\rm min}$ is already an indication of an excellent fit to the observational data. This best-fitting solution and map of residuals are also presented in the Hess diagrams of Fig. 7. Finally, the best-fitting SFR(t) is shown in the upper left panel of Fig. 8.

To evaluate the errors for all involved parameters, we first find the correspondence between the $\chi^2_{\rm min}$ value for each model and its confidence level. This correspondence was estimated simulating 100 synthetic CMDs generated with a number of stars equal to the observed CMD, using the best-fitting SFR(t) and its parameters as the input for the simulations. So, after recovering the SFH for this sample of synthetic CMDs, it was possible to build the $\chi^2_{\rm min}$ distribution and to establish the relation between their values and the confidence level.

In the $\chi^2_{\rm min}$ maps of Fig. 6, we superimposed the 68 % and 95 % significance levels for all the solutions for the Centre. Only for [M/H] values between -0.52 and -0.42 we have solutions within the 68 % significance level of the best solution. Based on this figure, we determine $(m-M)_0 = 18.57 \pm 0.07$ and $A_V = 0.26 \pm 0.05$ for the cluster Centre (with random errors at the 68 % significance level).

The left panel of Fig. 8 shows the SFR(t) for the cluster Centre together with error bars, as derived for the initial age resolution of $\Delta \log t = 0.05$ dex. The most basic feature in this plot is that the SFR(t) is clearly non-null for two age bins, spanning the $\log(t/\mathrm{yr})$ interval from 9.15 to 9.25 (ages from 1.41 to 1.78 Gyr). This result is not only valid for the best fitting model, but also across the entire 68 % significance level volume of the A_V vs. $(m-M)_0$ and [M/H] diagrams. Solutions within this volume are used to define the range of systematic errors, which is also depicted in the figure. Finally, we note that the two bins of non-null star formation are found even if we adopt less restrictive limits for the random errors, i.e. if we plot all solutions inside the 95 % significance level.

However, the very small random errors for the $\Delta \log t = 0.05$ dex solution clearly suggest that the data presents the potential for a more detailed determination of the age distribution. The middle panel of Fig. 8 shows the solution when we adopt 20 SPMs separated by $\Delta \log(\mathrm{age}) = 0.025$ dex, as obtained with the same data and methods, but for a fixed value of $(m-M)_0 = 18.57, A_V = 0.26$, [M/H] $= -0.49$. Now the solution is clearly non-null for 3 age bins, spanning the $\log(t/\mathrm{yr})$ interval from 9.175 to 9.25 (ages from 1.50 to 1.78 Gyr). As a result of the smaller number of stars per bin, random errors are larger than in the previous $\Delta \log t = 0.05$ dex case[4].

[4] Note that systematic errors are computed only in the case of

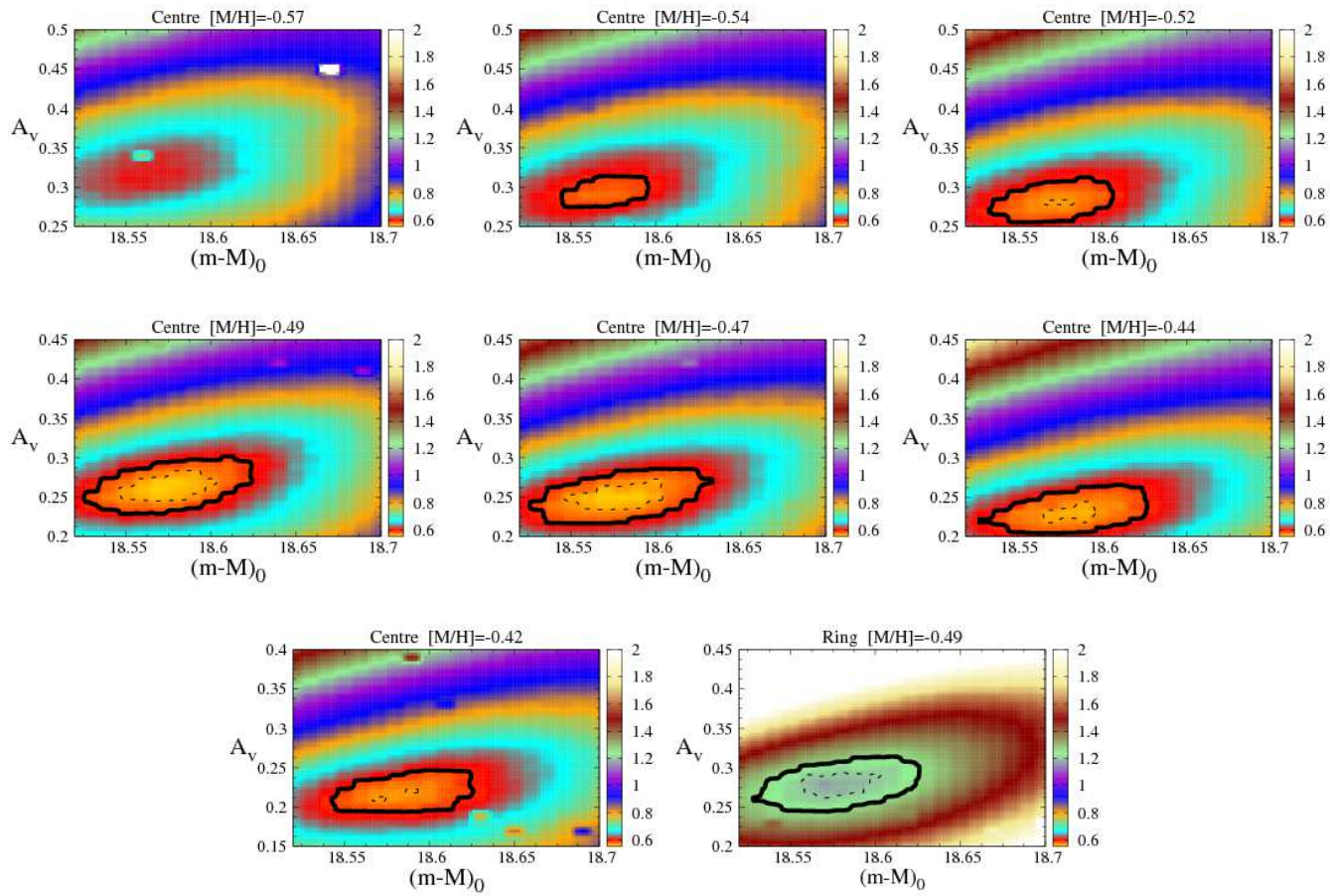

Figure 6. The **first 7 panels** show the maps of the $\chi^2_{\rm min}$ obtained from the SFH-recovery of the NGC 1846 Centre, as a function of $(m-M)_0$ and A_V, for several [M/H] values (from -0.57 to -0.42). The black lines delimit the regions within the 68 % (dashed lines) and 95 % confidence levels (continuous lines) of the absolute best solution, which is found at [M/H] $= -0.49$ and is shown in the fourth panel. The **last panel** shows the same for the NGC 1846 Ring, but only for the metallicity of [M/H] $= -0.49$. The minimum $\chi^2_{\rm min}$ are of 0.55 and 1.1, respectively, for the Centre and Ring. In both cases, the best-fitting solutions are found at $(m-M)_0 = 18.57$, $A_V = 0.26$.

We proceed with this experiment, determining the SFH for an even better age resolution, namely $\Delta \log t = 0.015$ dex. The results are in the right panel of Fig. 8. This time, the random errors are really large, as a consequence of the quite small number of stars per age bin. Under these conditions, the result of the SFH analysis could depend very much on the particular choice of limits for the age bins. In order to appreciate the SFR(t) for several bin positions (and always with the same resolution, of $\Delta \log t = 0.015$ dex), the age bins have been shifted progressively by steps equal to 1/5 of the total bin width, that is, by 0.003 dex. The right panel of Fig. 8 is the result of plotting all these results together as a function of the bin central age. The SFR(t) appears much more continuous than in previous cases, and presents clear indications about two points:

(i) The SFR(t) is non-null in the complete age interval from $\log(t/{\rm yr}) = 9.18$ to 9.25 (ages from 1.51 to 1.78 Gyr), which is in perfect agreement with the interval revealed by the SFR(t) of intermediate resolution, $\Delta \log t = 0.025$ dex.

(ii) There is a marked minimum in the SFR(t) for the age bins with $\log(t/{\rm yr})$ going from 9.22 to 9.23 (ages 1.66 to 1.70 Gyr). Despite the large error bars, this minimum is statistically significant. It indicates, surprisingly, that there might have been a hiatus in the SFR(t) of NGC 1846, starting ~ 150 Myr after the first episode of star formation, and lasting for about 50 Myr.

the default age resolution of $\Delta \log t = 0.05$ dex, for which we fully explored the possible interval of $(m-M)_0, A_V$, [M/H]. The basic reasons for not recomputing the systematic errors when adopting a better age resolution, are essentially: (1) The large CPU times needed to explore the entire $(m-M)_0, A_V$, [M/H] interval. (2) Test runs of our software indicate that the best-fitting values of these parameters depend little on the age resolution $\Delta \log t$ being adopted. Indeed, they are strongly constrained by the CMD portions corresponding to the lower main sequence, RGB, and main body of the red clump, which are equally well fitted at all age resolutions. Therefore, the systematic errors obtained at $\Delta \log t = 0.05$ dex shall be considered as indicative of those expected at all age resolutions.

3.3.2 The SFH for the NGC 1846 Ring

In the case of the NGC 1846 Ring we *assume* it has the same [M/H] as the cluster Centre, and explore the solutions in the

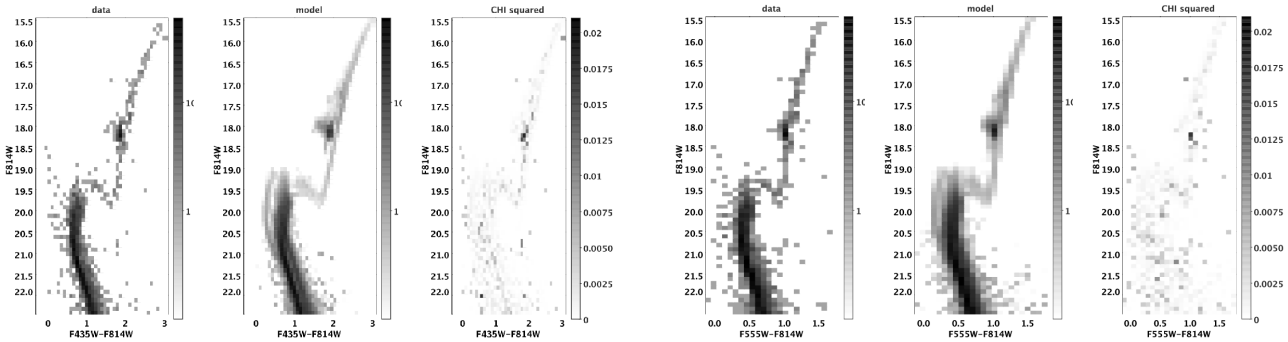

(a) Centre of NGC 1846

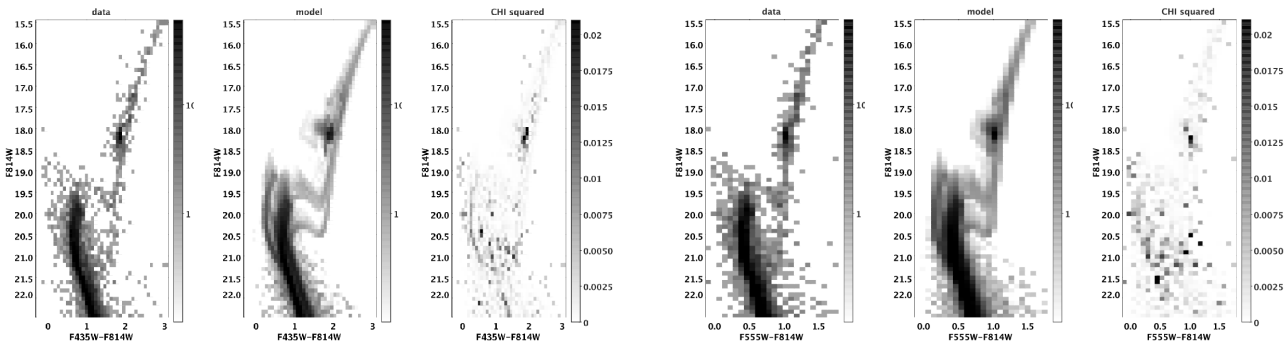

(b) Ring of NGC 1846

Figure 7. The Hess diagrams for the NGC 1846 Centre region (top panels) and Ring region (bottom panels). From left to right, the panels show the cluster F435W–F814W vs. F814W diagram, its best-fitting solution model, and the chi2 map. The same is done for the F555W–F814W vs. F814W diagram.

$(m-M)_0$ vs. A_V plane, as shown in the last panel of Fig. 6. The assumption of the same [M/H] is natural for stars belonging to the same (presumably chemically-homogeneous) cluster. In this case, the cluster Centre is taken as the reference because it suffers less from field contamination and differential reddening, which are two potential sources of systematic errors in the determination of [M/H]. Moreover, the cluster Centre presents low $\chi^2_{\rm min}$ values, which means very good overall solutions.

The best solution for the Ring turns out to be located at the same $(m-M)_0$ as the cluster Centre, and at virtually the same A_V, as shown in Fig. 6. Experiments of SFH recovery at varying age resolution, as performed for the Centre, were repeated in the Ring. Also these results turned out to be remarkably similar to the Centre ones, as revealed by the bottom row of Fig. 8. In particular, the hiatus in star formation at $\log(t/{\rm yr}) = 9.22$ is clearly present also in the Ring. We will further comment on this in Sect. 4.

3.3.3 The binary fraction and mass function in NGC 1846

Apart from the already-mentioned assumptions (constant [M/H], no differential reddening, etc.) our analysis also adopted SPMs built for a fixed value for the PDMF slope and fraction of unresolved binaries. The question arises whether our results can help to better constrain these parameters, and their possible radial variations within the clusters. We test this by varying these parameters while keeping the same $(m-M)_0$, A_V, and [M/H] as in the best-fitting solution. In order to be more sensible to differences in the PDMF slope, we now cut the CMDs at a limiting magnitude of F814W < 24.25 mag, which corresponds to main sequence stars with ~ 0.7 $M_\odot$. Needless to say, by going to deeper magnitudes we are also including CMD regions of smaller completeness and with higher photometric errors. Although

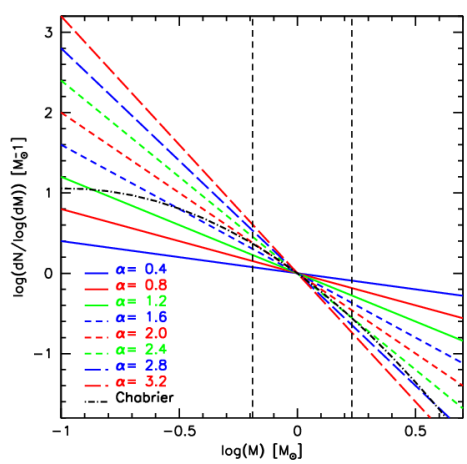

Figure 9. PDMFs used to derive the best-fit solutions for the clusters. The red, blue and green lines show the PDMF with 8 different slopes, α, from 0.4 to 3.6. The dot-dashed line shows the Chabrier (2001) PDMF previously used to recover the detailed SFHs for the clusters and their fields. The dashed vertical lines indicate the mass interval relevant to this work.

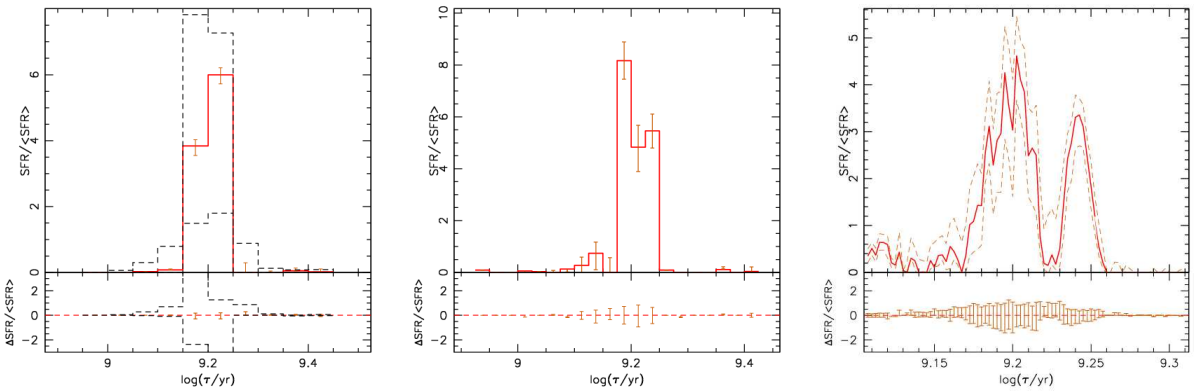

(a) SFR(t) for NGC 1846 Centre

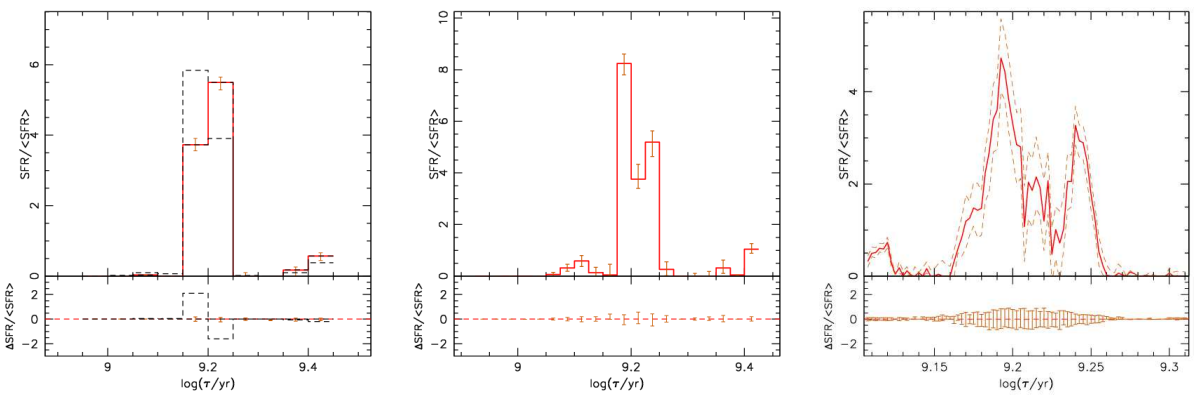

(b) SFR(t) for NGC 1846 Ring

Figure 8. Top row (a): The SFR(t) normalized to the average SFR over the complete age interval, for the NGC 1846 Centre, and derived for three different widths of the age bins, namely $\Delta \log t = 0.05, 0.025$ and 0.015 (from left to right, respectively). In the **leftmost panel**, the red histogram shows the SFR(t) for the best-fitting solution, while the orange bars show the random errors at the 68 % confidence level. The black dashed lines show the systematic errors inside the area of 68 % confidence level shown in Fig. 6. The **central panel** shows the same for a resolution twice as better, resulting on a more detailed SFR(t), but with random errors about twice as large. Finally, the **rightmost panel** shows the SFR(t) computed with a fixed resolution of $\Delta \log t = 0.015$, but moving the age bin centers at small steps of 0.003 dex in $\log t$, so that the SFR(t) appears more continuous – and indeed, we change the SFR(t) plot to use continuous lines instead of histograms, in order to better illustrate these particular results. The continuous red line is the SFR(t) while the dashed orange lines illustrate the interval of random errors, at the 68 % confidence level. **Bottom row (b):** The same for the NGC 1846 Ring region. To provide a better comparison between the error bars among the different cases, the **smaller sub-panels** at the bottom of each panel show the errors (random, and also systematic in the case of $\Delta \log t = 0.05$ dex) as referred to the mean SFR(t) line.

these processes are properly modelled by our ASTs, it is also true that the PDMF determinations we are doing here shall be considered of a more exploratory nature, than our previous determinations of the cluster SFHs.

The binary fraction is parametrized by the fraction f of detached binaries with a mass ratio in the interval from 0.7 to 1. These binaries cause the well-known sequence parallel to the main sequence in the CMD, while binaries with a smaller mass ratio leave hardly any signature in optical CMDs. The PDMF slope is parametrized by the Salpeter (1955) slope, α (with $dN/dM \propto M^{-\alpha}$), which changes the number ratio between the stars at and above the MSTO, and the fainter main sequence. PDMF slopes tested in this work are illustrated in Fig. 9. As a reference, the main sequence stars at F814W $\sim$24.25 mag, have $\sim$0.7 $M_{\odot}$. For the mass range of interest here, the Chabrier (2001) PDMF has a slope of $\alpha \simeq 2.2$.

In this exercise, we start from the best fitting solutions for an age resolution of 0.05 dex, and run StarFISH for all f and α combinations, for a fixed distance and reddening. The results are illustrated in the $\chi^2_{\rm min}$ map of Fig. 10, separately for the NGC 1846 Centre and Ring. In this figure, the $\chi^2_{\rm min}$ maps were normalized to the minimum value of $\chi^2_{\rm min}$, to allow a better comparison between our results. The best-fitting solutions are found for about the same values of α and f for both Centre and Ring: ($\alpha = 1.2, f = 0.15$) and ($\alpha = 1.6, f = 0.13$), respectively. Since we do not perform the error analysis, it is impossible to tell whether these small differences between Centre and Ring are statistically significant or not. Anyway, these values seem to indicate flatter PDMFs than the ones commonly found in galactic or extragalactic stellar clusters, which typically present PDMF slopes close to the Salpeter (1955, $\alpha = 2.35$) or Chabrier (2001, $\alpha \sim 2.2$) one (see also e.g. Kroupa 2001, 2002; Bastian, Covey & Meyer 2010).

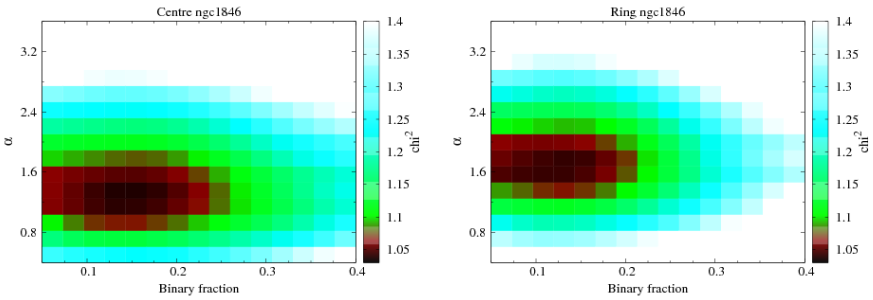

Figure 10. $\chi^2_{\rm min}$ map normalized to the minimum $\chi^2_{\rm min}$ for the NGC 1846 Centre (left panel) and the Ring (right panel) solutions, as a function of binary fraction f and PDMF slope α.

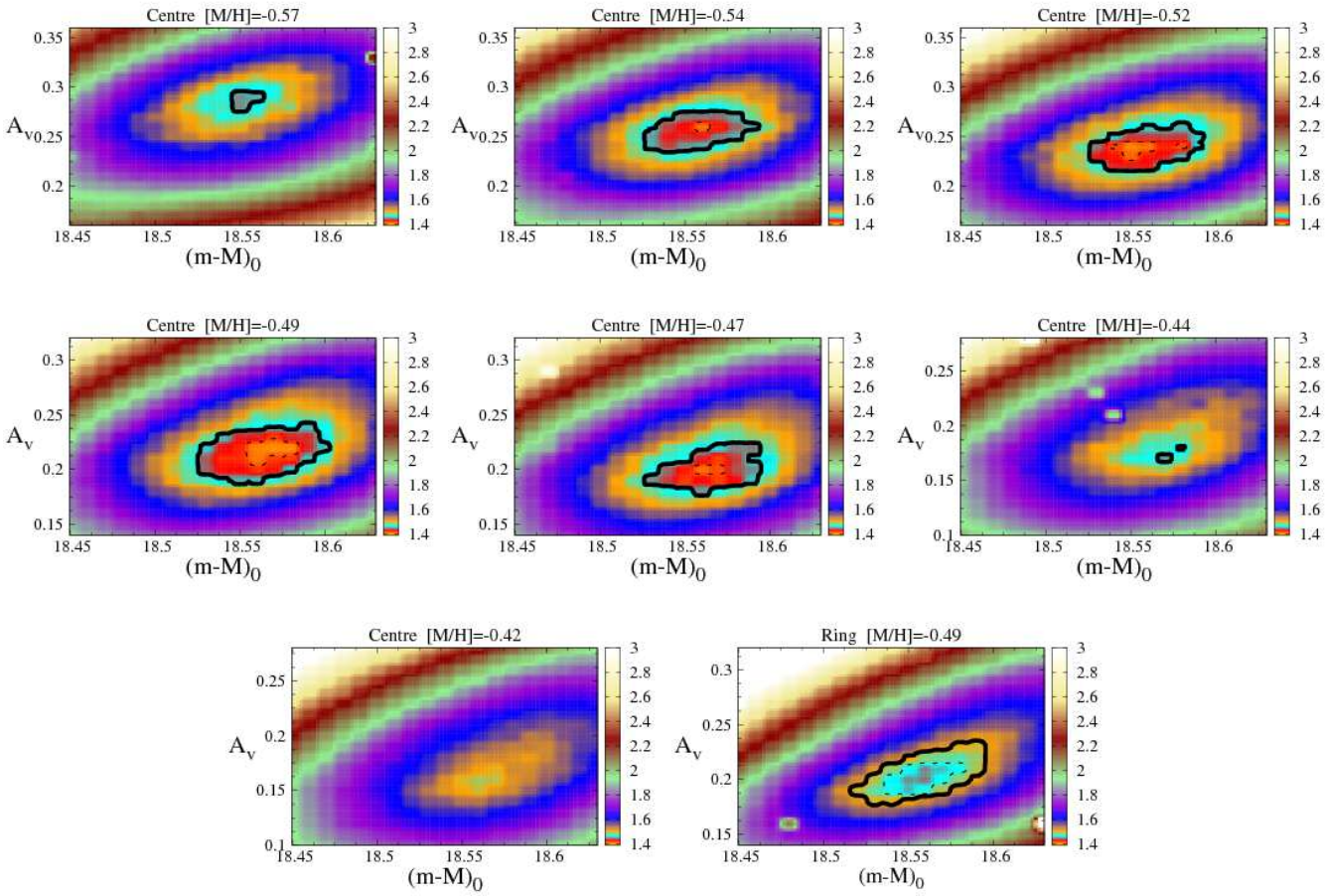

Figure 11. The same as Fig. 6 but for NGC 1783. The minimum $\chi^2_{\rm min}$ is of 1.39 and 1.45 for Centre and Ring, respectively.

3.3.4 The SFH of NGC 1783 Centre and Ring

We proceed in the analysis of NGC 1783 exactly in the same way as for NGC 1846. Complete maps of $\chi^2_{\rm min}$ for the Centre, as a function of $(m-M)_0$, A_V and metallicity, are presented in the first 7 panels of Fig. 11. The best solution is found again for [M/H] $= -0.49$, with $(m-M)_0 = 18.57$, $A_V = 0.22$, and a $\chi^2_{\rm min} = 1.39$. Solutions within the 68% confidence level span the range of metallicities between -0.47 and -0.54.

The metallicity of [M/H] $= -0.49$ turns out to coincide with the one previously determined for NGC 1846, which is not unexpected given their same ages. High resolution spectroscopy by Mucciarelli et al. (2008) instead indicates a value of [Fe/H] $= -0.35 \pm 0.02$.

Based on Fig. 11, we determine $(m-M)_0 = 18.57 \pm 0.07$ and $A_V = 0.22 \pm 0.05$ for the cluster Centre (with random errors at the 68 % significance level).

Using [M/H] $= -0.49$ for the Ring, we find good solutions in quite a similar region of the $(m-M)_0$ vs. A_V

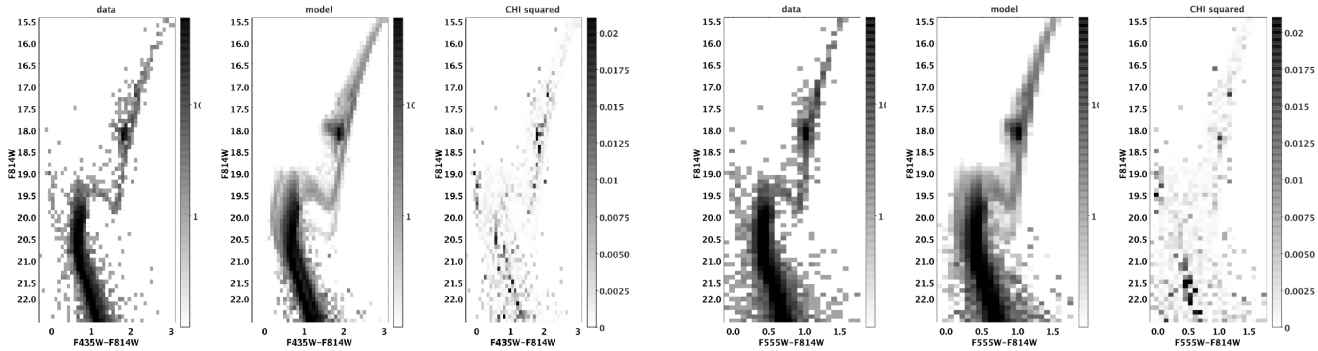

(a) Centre of NGC 1783

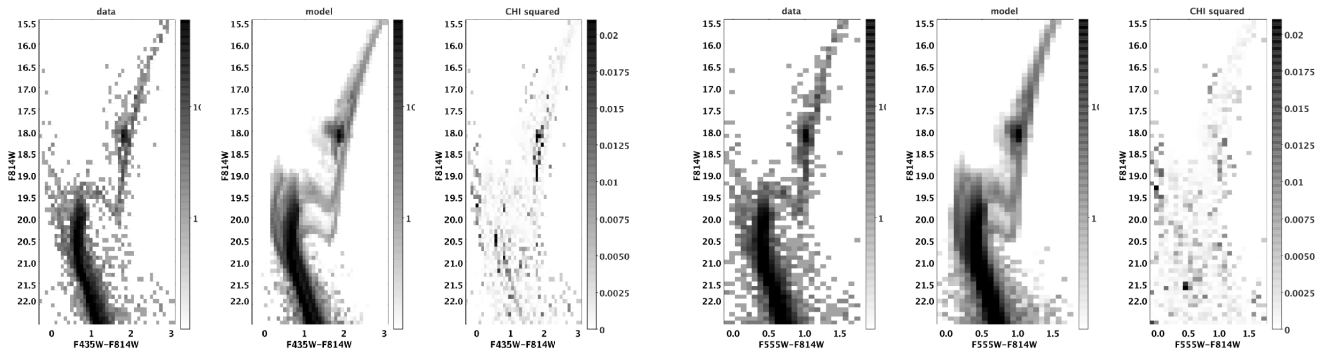

(b) Ring of NGC 1783

Figure 12. The same as Fig. 7 but for NGC 1783.

plane as for the Centre (see last panel in Fig. 11). The overall best solution is at $(m-M)_0 = 18.56$, $A_V = 0.20$, and has a $\chi^2_{\rm min} = 1.45$. We however take the solution at $(m-M)_0 = 18.57$ as the reference one, which presents a minimum $\chi^2_{\rm min}$ at $A_V = 0.22$ just as for the Centre. The best-fitting solutions and map of residuals are also presented in the Hess diagrams of Fig. 12, while the SFR(t) are illustrated in the left panels of Fig. 13.

The panels of Fig. 13 show the SFR(t) for the cluster Centre and Ring together with error bars, again at several different resolutions $\Delta \log t$. These solutions are remarkably similar to those already found for NGC 1846, in several aspects. Age intervals of non-null SFR(t) are essentially the same. In particular, also in NGC 1783 we find indication for a hiatus in the SFR(t) taking place ~ 150 Myr after the initial burst of star formation. Comparison between the middle panels of Fig. 13, however, reveals something new: the SFR(t) tends to be slightly older in the cluster Centre than in the Ring. In particular, the Ring seems to present a less marked peak of star formation at older ages.

To verify whether this difference could be due to an incorrect account of the field contamination in the NGC 1783 Ring region, we make an additional test, illustrated in Fig. 14: The contribution of the field is artificially increased/decreased by 50 %, with respect to the contribution expected for the Ring area, and then the SFH recovery is repeated. The results are almost indistinguishable from those in the bottom-right panel of Fig. 13, indicating that this is not the factor driving the different results between Center and Ring in NGC 1783.

3.3.5 The binary fraction and mass function in NGC 1783

As for NGC 1846, also for NGC 1783 we take the best-fitting solutions for Centre and Ring and vary its binary fraction f and PDMF slope α. The maps of $\chi^2_{\rm min}$ are presented in Fig. 15. The results this time appear noticeably different between Centre and Ring: While for the Centre the best-fitting values are $\alpha = 1.3$ and $f = 0.20$, for the Ring they are $\alpha = 2.0$ and $f = 0.15$. These values of α provide hints of a possible mass segregation in this cluster.

The interpretation of this finding is not straightforward. Due to CPU time limitations we did not perform a thorough exploration of the parameter space, neither the detailed analysis of random and systematic errors that would be required to define the significance of the detected PDMF variation. Anyway, we think the results are interesting enough to be mentioned here, considering the novelty of determining α in different regions of clusters with MMSTOs. Since we find a smaller contribution of the older stars in the Ring, the deficit of less massive stars in the Ring is more likely associated to the younger population.

4 DISCUSSION

Our analysis produces a number of results, that we now compare to previous results for the same clusters, and frame in the present scenarios for the production of multiple populations in Magellanic Cloud clusters.

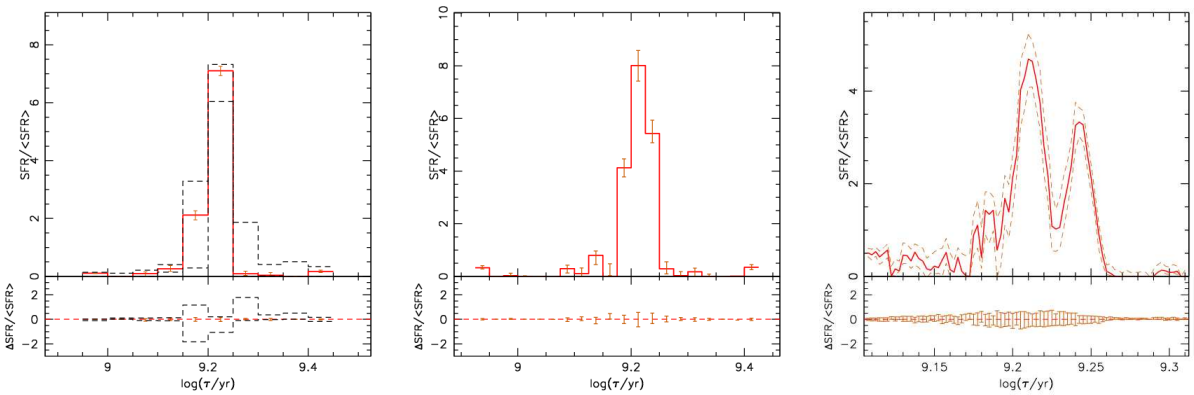

(a) SFR(t) for NGC 1783 Centre

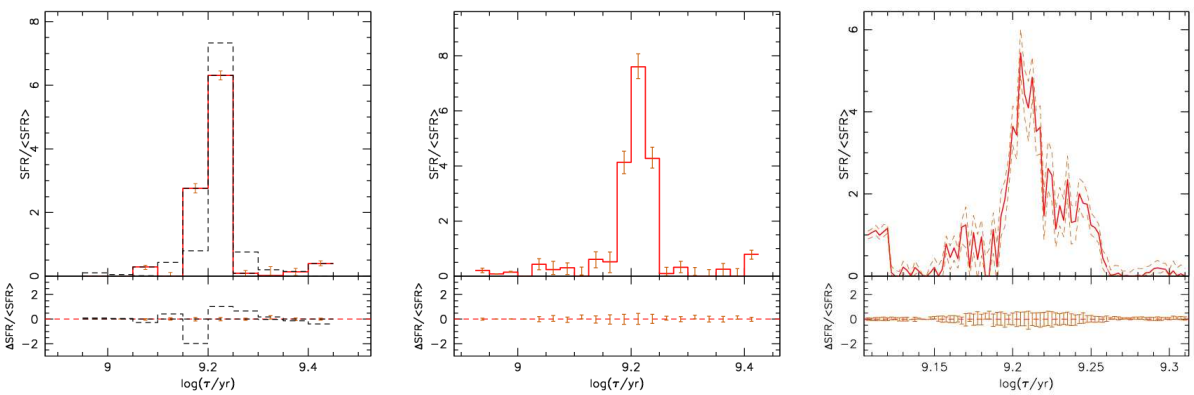

(b) SFR(t) for NGC 1783 Ring

Figure 13. The same as Fig. 8 but for NGC 1783.

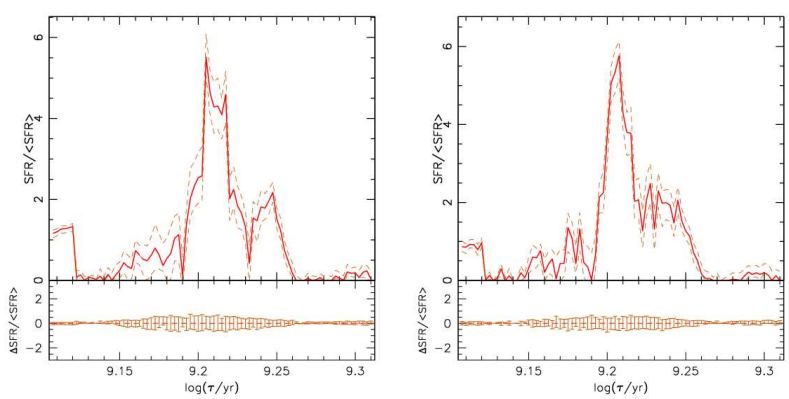

Figure 14. The high-resolution SFH derived for the NGC 1783 Ring, now assuming a field contamination decreased/increased by 50 % (left/right panels, respectively), with respect to the values expected for the Ring area.

4.1 Comparing the SFH between NGC 1846 and NGC 1783 Centres

As easily noticeable by comparing the top right panels of Figs. 8 and 13, the timescales for the SFH in NGC 1846 and NGC 1783 Centres are surprisingly similar. They both seem to have formed stars for a total period of about 0.3 Gyr. They both started the star formation activity in a marked burst peaked at $\log(t/\mathrm{yr}) = 9.24$ or 9.25 ($t = 1.78$ Gyr). The FWHM of this marked peak is, in both cases, of 0.02 dex in $\log t$, which is indistinguishable from the actual resolution of $\Delta \log t = 0.015$ dex of the SFH-recovery method. In both clusters, this strong peak is followed by a short hiatus in SFR(t), which lasts long enough to be detected by the method, that is, at least 0.02 dex in $\log t$ (or 70 Myr). Then the SFR(t) proceeds up to more recent times, becoming null at ages of $\log(t/\mathrm{yr}) = 9.17$ (1.48 Gyr). In the following, for obvious reasons we will refer to the marked peak observed in the SFR(t) as the *first generation*, and the extended period of star formation, after the hiatus, as the *second generation*.

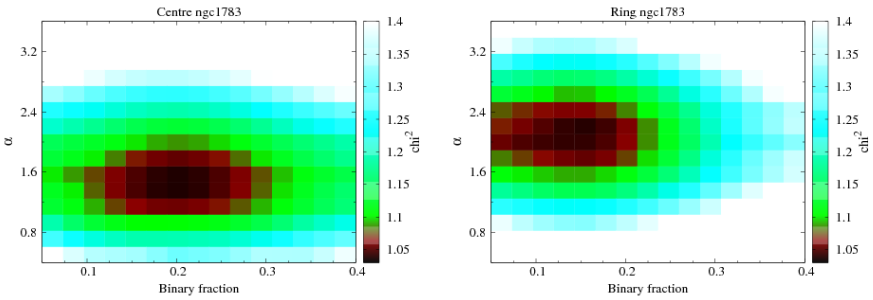

Figure 15. The same as Fig. 10, but for NGC 1783.

It should be clear however that more than two generations may be present, especially in the later periods of star formation (younger stellar ages).

The presence of separated periods of star formation in these clusters has been already advanced by other authors, using essentially the same set of HST images, but different data reductions and methods. Mackey & Broby Nielsen (2007), Mackey et al. (2008) and Milone et al. (2009) noticed that the MSTO region in NGC 1846 was clearly split or bimodal, hence suggesting the presence of two main populations separated in age. Goudfrooij et al. (2009, 2011b) instead derive a continuous distribution of stars across the MSTO region, hence concluding that the SFR(t) likely proceeded continuously over a period of $\sim$ 300 Myr. For NGC 1783, Mucciarelli, Origlia & Ferraro (2007) find no evidence of a broad turn-off, while Mackey et al. (2008) and Goudfrooij et al. (2011b) claimed a MMSTO with a smooth age distribution, whereas Milone et al. (2009) suggests a double MSTO. Our paper, instead, would agree more with the interpretation of a split MSTO in both clusters. Notice that the different results cannot be attributed to the different data reduction only. The main different between our analysis and the previous ones is in the fact that we use the information in the entire CMD, and not only the one across the MSTO, in order to derive the age distribution. Our method also attempts to fit other age-sensitive features like the subgiant branches and red clumps – very well drawn in the CMD of both clusters, see Fig. 3.

As already mentioned in Sect. 1, the most evident difference between NGC 1846 and NGC 1783 is in their different radii, while most of their other parameters are quite similar – including the total mass, mean metallicity, and level of contamination by the LMC disk. Both clusters are among the most massive of their ages in the LMC. It is not hard to imagine that they formed at about the same age, as a result of the same sort of dynamical process (or the same large-scale dynamical event) in the LMC. All the above-mentioned aspects point to a common process operating in a similar way in both clusters, from the onset of star formation up to later stages.

Among the scenarios advanced to explain prolonged star formation in LMC star clusters, two are particularly worth of being commented here: First, from dynamical arguments and the inferred escape velocity at an age of 10 Myr of several clusters exhibiting MMSTOs, Goudfrooij et al. (2011a) suggest that second-generation stars start being formed from cluster material shed by first-generation stars featuring slow stellar winds. In our results, the second generation appears after a period of time to be located between 160 and 220 Myr after the first generation. This time lag corresponds to the main-sequence lifetimes of stars with masses between 4.0 and 3.4 $M_{\odot}$, which are expected to quietly end their nuclear lives as mass-losing AGB stars with low-velocity winds ($\sim 15-20$ km s^{-1} ; Habing & Olofsson 2003). Thus, our results for the duration of the SFH hiatus are certainly compatible with Goudfrooij et al. (2011a)'s results.

A somewhat similar scenario has been advanced by Conroy & Spergel (2011), who suggest that the supernovae of type II and the prompt type Ia from the first-generation stars, first clean up the interstellar medium of the cluster; the interstellar medium is then reformed at the cluster centre as intermediate-mass stars start shedding their envelopes at ages larger than 100 Myr. The accumulated gas then cools as the Lyman-Werner photon flux from the cluster stars drops after a few 100 Myr, which allows molecular hydrogen and stars to form. This starts the second-generation of star formation, after which no third generation can follow because late SN Ia from the first generation clean up the cluster gas again. Although detailed in the description of the processes that can allow/interrupt star formation in clusters, Conroy & Spergel (2011)'s scenario do not make very precise predictions about the timescales of the different processes involved. Anyway, it is clear that our findings regarding the SFH, with the observation of first and second-generation stars, are also in agreement with their description. In addition, our observations indicate that in these $\sim 10^5$ $M_{\odot}$ clusters the final dissolution of the central interstellar medium by late SN Ia takes place after 0.3 Gyr. In the SMC cluster NGC 419, using the same method we find evidence for a total interval of star formation at least twice as long (Rubele, Kerber & Girardi 2010). These numbers may provide important constraints for a further refinement of the Conroy & Spergel (2011) scenario.

4.2 Comparing Centre and Ring SFHs

Another finding from our methods regards the similarities/differences between the SFHs at the cluster Centres and Rings. As indicated by the right panels in Figs. 8 and 13, we find hints of a different SFH between Centre and Ring for NGC 1783, in which the Ring has a much less pronounced

first-generation peak. For NGC 1846, instead, there is no suggestion of a similar effect.

This result is particularly surprising since results from Goudfrooij et al. (2011a), derived from the same data, seem to suggest exactly the opposite: after drawing boxes in the CMD for these and other clusters, they counts stars in the "upper and lower MSTO regions", finding that both kinds of stars present a very similar radial distribution in NGC 1783, while in NGC 1846 the upper MSTO stars are clearly more centrally concentrated.

As already commented, the present analysis uses all stars in the CMD, whereas Goudfrooij et al. (2011a) explicitly avoids dealing with background/field subtraction issues by excluding areas in the CMD where the background was found to contribute more than 20% to the star counts. Their goal is to deal with quite robust star counts as function of radius. Thus, Goudfrooij et al. (2011a) do not use a large part of the MS, and the top-left extreme of the MSTO, which instead are included in the present analysis. In addition, Goudfrooij et al. (2011a)'s method is model-independent.

Our approach instead aims to maximize the number statistics by including all stars irrespective of their origin, and, additionally, to limit the impact of subjective choices regarding the stars included in the analysis. This attempt cannot be free of subjective choices, however. For instance, we had to decide, quite subjectively, the extent of Centre and Ring regions. Also, we use a particular set of isochrones, under the implicit assumption that they accurately describe all relevant phases of stellar evolution. Inaccuracies in these isochrones would unavoidably appear as systematic errors in all of our results.

These contrasting results clearly make somewhat uncertain any attempt to use the radial trend to discuss the scenario for the formation of second-generation in these clusters. Formally speaking, the results for NGC 1846 – no difference between Centre and Ring SFH – seem just to indicate that we were not able, with our definition of Centre and Ring, to detect the expected concentration of the second generation towards the centre of this cluster. This is not surprising. What is surprising is the trend derived for NGC 1783, which would suggest that, in less concentrated clusters like this, second-generation stars are spatially more spread than first-generation ones. No scenario for the formation of multiple populations in clusters seem to favour such a trend. This point clearly deserves more accurate analysis.

As for the determination of the PDMF and binary fractions, the basic results is that we find hints of mass segregation in NGC 1783, at a level which is certainly larger than in NGC 1846, but which, however, may not be statistically significant. NGC 1783 is also the cluster with the largest radius, the larger concentration index c, and also the one for which Centre and Ring seem to present a different SFR(t). It is tempting to suggest a correlation between all these different aspects, but any conclusion on this is hampered by the uncertainties in our determinations of α and f, in the determination of c for NGC 1783 (Goudfrooij et al. 2011b), and on the fact that we have analysed just two clusters. It would be very interesting to extend the same kind of determination to a much larger sample.

At first sight, our clusters seem to follow the anti-correlation between the concentration index c and the slope of the global mass function, which is detected in Galactic globular clusters (GGCs ; De Marchi, Paresce & Pulone 2007) and interpreted as the result of residual-gas expulsion in initially mass-segregated star clusters (Marks, Kroupa & Baumgardt 2008): indeed, we find the steepest mass function (larger α) in NGC 1783, the cluster with the larger concentration index. We can also confirm that, after taking into account the different definitions of c and α (i.e. the use of logarithm for c, and the multiplication by -1 in the case of α) by different authours, we find values comparable to those derived by Glatt et al. (2011) for 6 SMC intermediate-age and old clusters; these values place them from ~ 2 to 3 dex bellow the α vs. c relation typical of GGCs. The interpretation of these trends is not easy, since all these clusters have been analysed using different methods and heterogeneous data, and, moreover, the mean De Marchi, Paresce & Pulone (2007)'s relation is usually derived for entire clusters, and not for different cluster regions as in our case.

4.3 Concluding remarks

Together with our previous findings for the SMC clusters NGC 419 (Rubele, Kerber & Girardi 2010) and NGC 1751 (Rubele et al. 2011) using the same techniques, the present results for NGC 1846 and NGC 1783 confirm that multiple episodes of star formation provide a good quantitative description of the observed CMD features. At this point, research in the field should concentrate on carefully age-dating the different populations, and in identifying features that can favour/disfavour the possible scenarios for their formation. In this sense, the present work has been partially successful. Without imposing any a priori limitation or preselected shape to the SFH, we have found the presence of separated first and second-generation episodes of SFH for both clusters. This observation is compatible with simple schemes where second-generation SFR(t) can only start after a period of a few 100 Myr, when the prompt supernovae and the Lyman-Werner flux from first-generation stars are over (Conroy & Spergel 2011). The stellar ejecta accumulated to form the second-generation should come partially from 3.4–4.0 $M_{\odot}$ stars of the first generation, and be shed through slow AGB winds, in accordance with the correlation between the presence of MMSTOs and $v_{\rm esc}$ at an age with 10 Myr found by Goudfrooij et al. (2011a).

However, we find an intriguing central concentration of first-generation stars in the cluster NGC 1783, which is opposite to what predicted by the above-mentioned scenarios. This cluster has a large core radius and concentration index, which may be associated with the observed gradients in the stellar population. The bad definition of the cluster field does not seem responsible for the observed trends, because the field contribution is anyway very small. However, clarification of this issue may requires the analysis of larger areas around the cluster, and of more clusters of similar age and different structural parameters. These steps will be pursued in subsequent papers.

ACKNOWLEDGMENTS

VKP is grateful to Jay Anderson for sharing his ePSF program. We acknowledge the anonymous referee for the many

suggestions that greatly helped us to improve the text. The data presented in this paper were obtained from the Multimission Archive at the Space Telescope Science Institute (MAST). STScI is operated by the Association of Universities for Research in Astronomy, Inc., under NASA contract NAS5-26555.

REFERENCES

Anderson J. et al., 2008, AJ, 135, 2055
Bastian N., Covey K. R., Meyer M. R., 2010, ARA&A, 48, 339
Bastian N., de Mink S. E., 2009, MNRAS, 398, L11
Bressan A., Marigo P., Girardi L., Salasnich B., Dal Cero C., Rubele S., Nanni A., 2012, MNRAS, 427, 127
Bressan A. G., Chiosi C., Bertelli G., 1981, A&A, 102, 25
Caffau E., Ludwig H.-G., Steffen M., Freytag B., Bonifacio P., 2011, Sol. Phys., 268, 255
Carrera R., Gallart C., Hardy E., Aparicio A., Zinn R., 2008, AJ, 135, 836
Chabrier G., 2001, ApJ, 554, 1274
Conroy C., Spergel D. N., 2011, ApJ, 726, 36
De Marchi G., Paresce F., Pulone L., 2007, ApJ, 656, L65
Dolphin A. E., 2002, MNRAS, 332, 91
Elson R. A. W., 1992, MNRAS, 256, 515
Gallart C., Freedman W. L., Aparicio A., Bertelli G., Chiosi C., 1999, AJ, 118, 2245
Girardi L., Chiosi C., Bertelli G., Bressan A., 1995, A&A, 298, 87
Girardi L. et al., 2008, PASP, 120, 583
Girardi L., Eggenberger P., Miglio A., 2011, MNRAS, 412, L103
Girardi L., Groenewegen M. A. T., Hatziminaoglou E., da Costa L., 2005, A&A, 436, 895
Girardi L., Rubele S., Kerber L., 2009, MNRAS, 394, L74
Glatt K. et al., 2011, AJ, 142, 36
Goudfrooij P., Puzia T. H., Chandar R., Kozhurina-Platais V., 2011a, ApJ, 737, 4
Goudfrooij P., Puzia T. H., Kozhurina-Platais V., Chandar R., 2009, AJ, 137, 4988
—, 2011b, ApJ, 737, 3
Grocholski A. J., Cole A. A., Sarajedini A., Geisler D., Smith V. V., 2006, AJ, 132, 1630
Habing H. J., Olofsson H., eds., 2003, Asymptotic giant branch stars
Harris J., Zaritsky D., 2001, ApJS, 136, 25
—, 2004, AJ, 127, 1531
—, 2009, AJ, 138, 1243
Haschke R., Grebel E. K., Duffau S., 2011, AJ, 141, 158
Holtzman J. A. et al., 1999, AJ, 118, 2262
Javiel S. C., Santiago B. X., Kerber L. O., 2005, A&A, 431, 73
Keller S. C., Mackey A. D., Da Costa G. S., 2011, ApJ, 731, 22
Kerber L. O., Santiago B. X., Brocato E., 2007, A&A, 462, 139
Kroupa P., 2001, MNRAS, 322, 231
—, 2002, Science, 295, 82
Lebzelter T., Lederer M. T., Cristallo S., Hinkle K. H., Straniero O., Aringer B., 2008, A&A, 486, 511
Mackey A. D., Broby Nielsen P., 2007, MNRAS, 379, 151
Mackey A. D., Broby Nielsen P., Ferguson A. M. N., Richardson J. C., 2008, ApJ, 681, L17
Marks M., Kroupa P., Baumgardt H., 2008, MNRAS, 386, 2047
Milone A. P., Bedin L. R., Piotto G., Anderson J., 2009, A&A, 497, 755
Mucciarelli A., Carretta E., Origlia L., Ferraro F. R., 2008, AJ, 136, 375
Mucciarelli A., Origlia L., Ferraro F. R., 2007, AJ, 134, 1813
Nikolaev S., Drake A. J., Keller S. C., Cook K. H., Dalal N., Griest K., Welch D. L., Kanbur S. M., 2004, ApJ, 601, 260
Olsen K. A. G., 1999, AJ, 117, 2244
Platais I. et al., 2012, ApJ, 751, L8
Riess A., Mack J., 2004, Time Dependence of ACS WFC CTE Corrections for Photometry and Future Predictions. Tech. rep., Space Telescope Science Institute
Ripepi V. et al., 2012, MNRAS, 3283
Rubele S., Girardi L., Kozhurina-Platais V., Goudfrooij P., Kerber L., 2011, MNRAS, 414, 2204
Rubele S., Kerber L., Girardi L., 2010, MNRAS, 403, 1156
Rubele S. et al., 2012, A&A, 537, A106
Salpeter E. E., 1955, ApJ, 121, 161
Smecker-Hane T. A., Cole A. A., Gallagher, III J. S., Stetson P. B., 2002, ApJ, 566, 239
van der Marel R. P., Alves D. R., Hardy E., Suntzeff N. B., 2002, AJ, 124, 2639
van der Marel R. P., Cioni M.-R. L., 2001, AJ, 122, 1807
Zaritsky D., Harris J., Thompson I. B., Grebel E. K., 2004, AJ, 128, 1606